Effect of Nanoclay on the Morphology and Properties of Poly(methyl methacrylate)/High-Density Polyethylene Blends

Sumana Mallick, Anup K. Dhibar, B. B. Khatua

Materials Science Centre, Indian Institute of Technology at Kharagpur, Kharagpur 721 302, India

Received 11 June 2009; accepted 16 September 2009
DOI 10.1002/app.31444
Published online 17 December 2009 in Wiley InterScience (www.interscience.wiley.com).

ABSTRACT: The effect of nanoclay on the morphology and properties of poly(methyl methacrylate) (PMMA)/high-density polyethylene (HDPE) blends was studied. A scanning electron microscopy study of the PMMA/HDPE (70/30 w/w) blends with nanoclay indicated a reduction in the average domain sizes of the dispersed HDPE phase and, hence, a better extent of mixing compared to that of the blends without any nanoclay. An X-ray diffraction study and transmission electron microscopy revealed the localization of intercalated nanoclay in the PMMA matrix of the PMMA/HDPE (70/30 w/w) blend. However, the same effect of clay was not observed in the PMMA/HDPE (30/70 w/w) blend when HDPE became the matrix. In the PMMA/HDPE (30/70 w/w) blend, the addition of nanoclay increased the domain size of the dispersed PMMA domains by preferential location of the clays inside the PMMA domains. The addition of polyethylene-grafted maleic anhydride in both compositions of the PMMA/HDPE blend effectively reduced the domain size of the disperse phases in the blend. However, the presence of clay increased the tensile strength and storage modulus of the PMMA/HDPE blends in both blend compositions. Thus, in the PMMA/HDPE blend, the clay platelets acted as a effective compatibilizer as long as they were dispersed mainly in the matrix phase. © 2009 Wiley Periodicals, Inc. J Appl Polym Sci 116: 1010–1020, 2010

Key words: compatibilization; nanocomposites; matrix

INTRODUCTION

Over the past several decades, the blending of conventional polymers has become a traditional method for producing new, high-performance polymeric materials. However, because of the immiscibility of polymers associated with their inherent thermodynamic incompatibility, most polymer blends tend to phase separate, which results in poor mechanical properties. The properties of multiphase polymeric materials are determined by the properties of the component polymers and the microstructure in the blend. Therefore, controlling the microstructure becomes a key factor in determining the performance of polymer blends. Traditionally, an effective way to attain satisfactory performance in incompatible polymer blends is to minimize the interfacial tension and to increase the interfacial adhesion. The use of a block or graft copolymer during processing plays an important role by causing entanglements or bridging different polymer chains near the interface.[1–6]

In recent years, polymer–clay nanocomposites have received a great deal of attention because of the realization that nanocomposites exhibit gains in structural, thermal, and mechanical properties without a significant loss in impact or clarity.[7] Many researchers have already reported the preparation and characterization of polymer–clay nanocomposites based on single-polymer matrices.[8–17] Recently, several groups have shown that nanoclay acts as a compatibilizer in immiscible polymer blends.[18–32]

Hong et al.[18] showed the effect of organoclay on the morphology of a poly(butylene terephthalate)/polyethylene blend. The location of clay in the specific phases with a certain amount of clay at the interface changed the viscosity ratio of the polymers in the blend and the blend morphology. Gelfer et al.[19] reported a reduction in the dispersed domain size (D) of a polystyrene (PS)/poly(methyl methacrylate) (PMMA) blend in the presence of organoclay. Wang et al.[20] reported that D of PS in a polypropylene (PP)/PS blend was greatly reduced by the addition of organoclay. Sinha Ray and coworkers[21–24] reported the role of nanoclay in various immiscible polymer blend systems. The presence of organoclay in immiscible polycarbonate/PMMA blends prevented the deformation of the dispersed phase,

Correspondence to: B. B. Khatua (khatuabb@matsc.iitkgp.ernet.in).

Contract grant sponsor: Indian Department of Science and Technology.

which enhanced the miscibility between the blend components.[21,22] The location of intercalated clay silicate layers at the interface decreased the interfacial tension and dispersed-phase particle sizes in immiscible PP/PS blend system.[23] A decrease in the viscosity ratio of PP and poly(butylene succinate) by selective localization of intercalated clay silicate layers in the poly(butylene succinate) phase changed the morphology of a PP/poly(butylene succinate) blend from highly phase-separated to a typical cocontinuous structure.[24] Khatua et al.[25] reported the role of exfoliated clay platelets on the morphology of nylon 6/poly(ethylene-*ran*-propylene) rubber blends. The selective dispersion of exfoliated silicate layers at the matrix phase decreased the average D values of the dispersed poly(ethylene-*ran*-propylene) rubber phase. Gcwabaza et al.[26] showed that the addition of 1.5 wt % organoclay in PP/poly(butylene succinate) blends resulted in the uniform dispersion of very fine particles of the dispersed phase. They assumed that intercalation of both the polymer chains into the same silicate stack at the interface and the effects of clay on the viscosity ratio were responsible for this improved morphology. Martins et al.[27] reported the lamellar morphology of the ethylene vinyl acetate phase in PP/ethylene vinyl acetate/clay nanocomposites when organoclay was selectively dispersed in the ethylene vinyl acetate phase with a fraction of exfoliated clay layers at the interface. Baghaei et al.[28] showed that addition of 5 wt % organoclay in a low-density polyethylene/ethylene–octene copolymer blend led to a reduction in the size of the ethylene–octene copolymer dispersed phase. Calcagno et al.[29] showed that the presence of montmorillonite in the poly(ethylene terephthalate) phase increased D of PP/poly(ethylene terephthalate) blends. Li and Shimizu[30,31] showed the formation of a cocontinuous structure in poly(phenylene oxide)/polyamide 6 and polyamide 6/acrylonitrile–butadiene–styrene blends in the presence of higher clay loading. Filippone et al.[32] also reported the formation of a cocontinuous phase morphology in a high-density polyethylene (HDPE)/polyamide 6 blend in the presence of 5 phr organoclay.

In summary, the literature contains reports on the effect of nanoclay on the morphology of several immiscible blend systems. Our objective was to investigate the effect of a small amount of clay on the morphology and properties of immiscible polymer blends where the clay layers were selectively located either in the matrix or in the dispersed phase. Thus, PMMA/HDPE (70/30 and 30/70 w/w) blends with different amounts of nanoclay (Cloisite 20A) and polyethylene-grafted maleic anhydride (PE-*g*-MA) were prepared via melt blending. Our main reason for choosing the PMMA/HDPE blend was that nanoclay could be selectively dispersed in the PMMA phase because of the difference in polarity between PMMA and HDPE. We discuss the details of our findings on the blend morphology, considering the location of the clays in the blends and comparing the results obtained by using PE-*g*-MA as a reactive compatibilizer.

EXPERIMENTAL

Materials

Commercial-grade PMMA (Gujpol 876G with a weight-average molecular weight of 95,000 and a melt flow index of 6 g/10 min and Gujpol 932HR with a weight-average molecular weight of 110,000 and a melt flow index of 2.2 g/10 min) was procured from GSFC (Gujrat, India). Gujpol 876G and Gujpol 932HR are called PMMA and PMMA-h, respectively, in this article. HDPE (M5018L) was obtained from Haldia Petrochemicals (Haldia, India). PE-*g*-MA (A-C 575P) was purchased from Honeywell (USA). Cloisite 20A, a modified montmorillonite, was supplied by Southern Clay Products, Inc. It was a montmorillonite modified with dimethyl dihydrogenated tallow ammonium to increase the layer spacing (d) of Na^+-montmorillonite. The cation-exchange capacity of Cloisite 20A was 95 mequiv/100 g. Hereafter, Cloisite 20A is referred to as the nanoclay.

Preparation of the blends

Blends of PMMA/HDPE (70/30 and 30/70 w/w) with various amounts (0–5 phr) of PE-*g*-MA and clay were prepared by melt mixing at 210°C and 60 rpm for 20 min in an internal mixture (Brabender Plasticorder, S.C. Dey & Co., Kolkata, India) with a capacity of 50 cc. To avoid moisture-induced thermal degradation, all polymers and the clay were completely dried in a vacuum oven at 80°C for 36 h before melt blending. Finally, the blends were compression-molded in a hot press at 210°C under a constant pressure (20 MPa) for further characterization.

Characterization

Scanning electron microscopy (SEM) study

The phase morphology of the PMMA/HDPE blends was studied with a scanning electron microscope (Vega II LSU, Tescan, Czech Republic), operated at an accelerating voltage of 5 kV. The specimens were carefully broken under a liquid nitrogen atmosphere. Then, the specimens were coated with a thin layer of gold to prevent electrical charging, and SEM images were taken of the fractured surfaces.

The number-average domain diameter (D_n) was obtained with Scion Image analyzer software (Scion Corp.). The cross-sectional area of each domain (A_i)

in the SEM micrograph was measured and then converted into the diameter of a circle with the same cross-sectional area (D_i) with the following equations:

$$D_i = 2(A_i/\pi)^{1/2} \quad (1)$$

$$D_n = \frac{\sum N_i D_i}{\sum N_i} \quad (2)$$

where N_i is the number of dispersed domains in the SEM micrograph.

X-ray diffraction study

The *d*-spacing of the layer structure of the clay itself and that in PMMA/HDPE blends was examined with a wide-angle X-ray diffractometer (Ultima III, Rigaku Corporation, Tokyo, Japan) with a nickel-filtered Cu Kα line (wavelength = 0.15404 nm), operated at 40 kV and 100 mA, at a scanning rate of 0.5°/min. The sample-to-detector distance was 400 mm.

Transmission electron microscopy (TEM) analysis

The location of the clay particles in the PMMA/HDPE blends was studied by TEM (JEM-2100, JEOL, Tokyo, Japan) at an accelerating voltage of 200 kV. The blend–clay nanocomposite samples were ultramicrotomed at cryogenic conditions with a thickness of 60–80 nm. Because the clay had a much higher electron density than the neat polymers, it appeared dark in the TEM images.

Complex viscosity measurement

A frequency sweep experiment for neat PMMA, HDPE, and the PMMA/HDPE blends without and with clay was done at 210°C under a nitrogen environment with an Advanced Rheometrics Expansion System (AR-1000, TA Instruments, Inc., New Castle, DE) with parallel plates 25 mm in diameter. The strain amplitude was 0.03, which was in the linear viscoelastic regime.

Dynamic mechanical analysis

The thermomechanical properties (storage modulus) of the compression-molded blends were measured in tension film mode at a constant vibration frequency of 1 Hz, a temperature range of 30–130°C, and a heating rate of 5°C/min in a nitrogen atmosphere with a dynamic mechanical analyzer (2980 model, TA Instruments, Inc.). The dimensions of the specimen were 30 × 6.40 × 0.45 mm^3.

Mechanical tests

Tensile measurements were carried out with a universal tensile testing machine (Hounsfield HS 10KS, UK) at room temperature with an extension speed of 5 mm/min and an initial gauge length of 35 mm. Dumbbell-shaped testing samples (64 × 12.7 × 3.2 mm^3) were used for tensile testing with at least 24 h allowed after molding to relax the stresses induced during cooling. The results reported are the averages of five samples for each composite, each with an experimental error of ±2%.

Thermogravimetric analysis (TGA)

The thermal stability (onset degradation temperature and temperature corresponding to 50% maximum weight loss) of the blends without and with the clay was investigated with TGA (TGA-209F, Netzsch, Germany). The sample was heated in an air atmosphere from room temperature to 600°C at a heating rate of 10°C/min.

RESULTS AND DISCUSSION

Morphological analysis

SEM images of the PMMA/HDPE (70/30 w/w) blends with various amounts of clay are shown in Figure 1. As observed, the HDPE phase in the PMMA/HDPE blend was dispersed as larger domains [Fig. 1(a)]. The addition of a small amount (0.5 phr) of nanoclay in the blend reduced *D* of the dispersed phase significantly [Fig. 1(b)]. As the amount of the clay was increased, *D* of the dispersed phase in the blend gradually decreased, although the decrease rate was much smaller [Fig. 1(c,d)]. This indicated that the nanoclay played an important role in reducing *D* of the dispersed phase of the PMMA/HDPE blends.

We also prepared PMMA/HDPE (70/30 w/w) blends with different amounts of PE-*g*-MA as a reactive compatibilizer to compare the decrease in *D* of the dispersed phase in the blends. From the SEM images (Fig. 2), a decrease in *D* of the dispersed phase in the blend was observed with increasing amount of PE-*g*-MA. However, the morphology of the PE-*g*-MA containing (up to 1 phr) blend was totally different compared to that of the blend with the same amount of clay [Fig. 1(b,c)]. For instance, the dispersed HDPE domains were more uniform in shape and size in the PMMA/HDPE (70/30 w/w) blend in the presence of 0.5 phr clay. We assumed that the increased viscosity of the PMMA matrix in the presence of clay and the barrier effect of the intercalated clay silicates effectively prevented the coalescence of HDPE domains at an early stage of melt mixing, whereas in the blend with PE-*g*-MA, the coalescence of HDPE domains was not restricted until PE-*g*-MA was located at the interface. Thus, the coalescence of HDPE domains, to some extent,

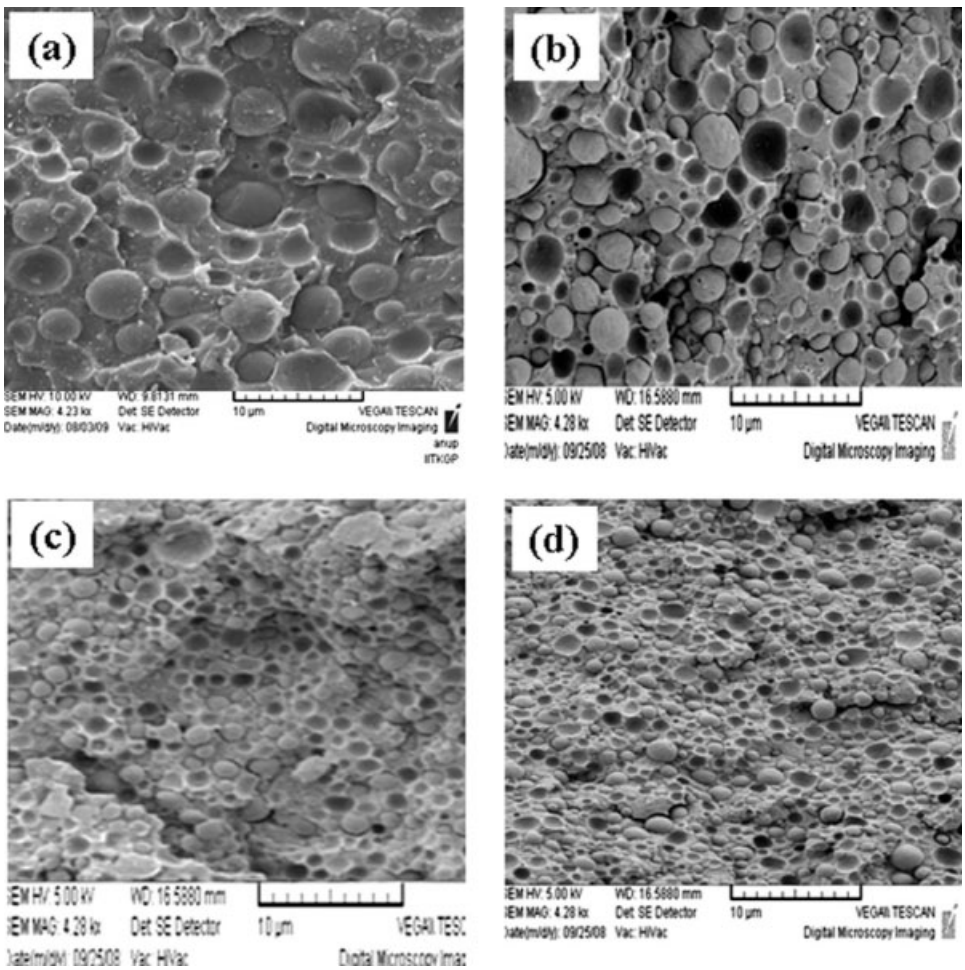

Figure 1 SEM images of PMMA/HDPE (70/30 w/w) blends with different loading levels of clay: (a) 0, (b) 0.5, (c) 1, and (d) 3 phr.

before the location of small amounts (0.5 and 1 phr) of PE-*g*-MA at the interface of the polymers, resulted in the formation of dispersed domains with different sizes in the blend. However, at a higher loading level (3 phr) of PE-*g*-MA, the blend revealed a morphology similar to the blend–clay system.

On the basis of SEM images, plots of D_n versus the amount of the clay and PE-*g*-MA are shown in

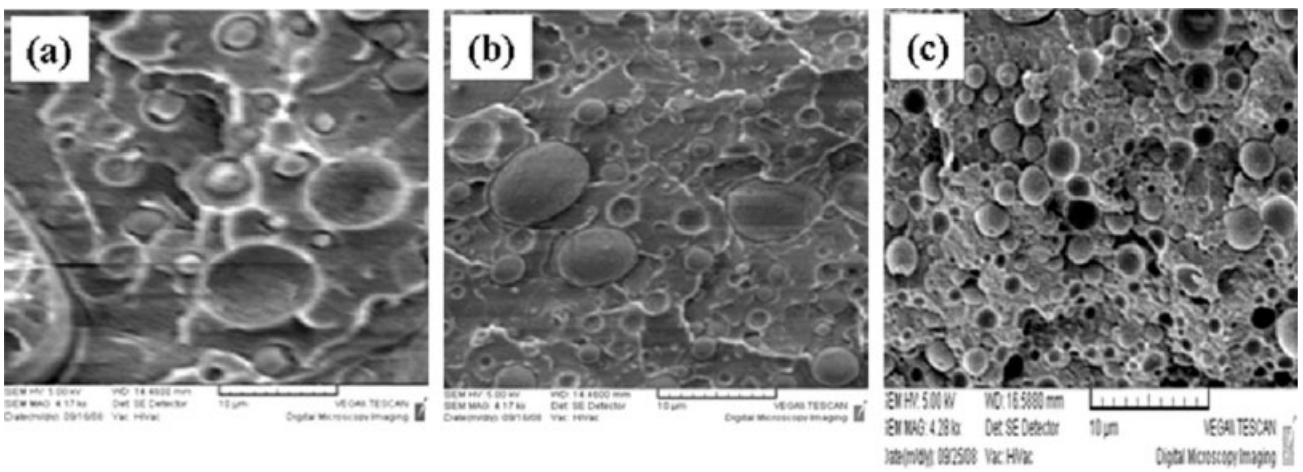

Figure 2 SEM images of PMMA/HDPE (70/30 w/w) blends with different amounts of PE-*g*-MA: (a) 0.5, (b) 1, and (c) 3 phr.

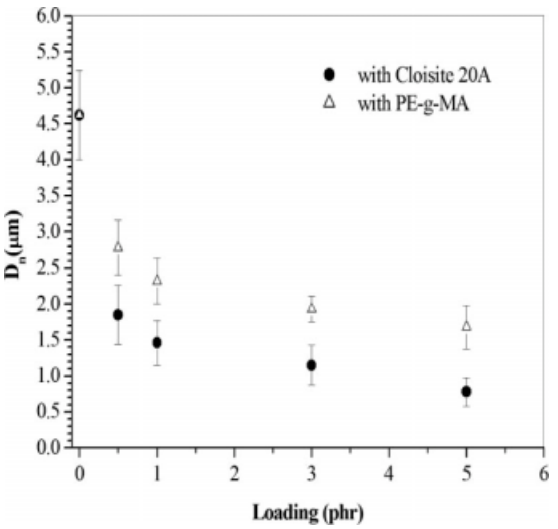

Figure 3 Plot of D_n versus various amounts of clay and PE-*g*-MA.

Figure 3. A rapid decrease in *D* of the dispersed phase in the blend was found at lower amounts of the clay, and then, a slow but gradual decrease in *D* of the dispersed phase in the blend was observed with further increasing amount of the clay. This curve was similar to the emulsification curve that has been reported for an immiscible blend with a block or graft copolymer.[33] The decrease in D_n of the dispersed HDPE phase with various amounts of the clay, shown in Figure 3, was very similar to that of the PMMA/HDPE (70/30 w/w) blend with various amounts of PE-*g*-MA as a reactive compatibilizer. However, the decrease in D_n of HDPE was relatively higher with the addition of clay than that with PE-*g*-MA.

Figure 4 shows the wide-angle X-ray diffraction profiles of the clay itself and its nanocomposites with PMMA, HDPE, and the PMMA/HDPE (70/30 w/w) blend. The clay itself exhibited a characteristic peak at a 2θ of 3.60°, corresponding to a *d*-spacing of 24.52 Å. The shifting of the clay peak position to a lower 2θ region in the PMMA/clay (2.38°) and HDPE/clay (2.98°) nanocomposites indicated the intercalation of PMMA and HDPE chains inside the clay galleries with *d*-spacings of 37.09 and 29.62 Å, respectively. The relatively higher extent of intercalation in the PMMA–clay nanocomposites was due to the difference in polarity between PMMA and HDPE. Interestingly, the characteristic peak for the clay at a 2θ of 2.37° in the PMMA/HDPE (70/30 w/w) blend with clay (1 phr) indicated the intercalation of the clay layers by PMMA chains only. This preferential location of clay in PMMA was due to the difference in polarity of PMMA and HDPE. Thus, the clay platelets were mostly located in the PMMA phase. However, a small amount of clay could be assumed to disperse at the interface.

The location of the clay platelets in the blend–clay nanocomposites was investigated by TEM analysis. Figure 5 represents the TEM images of the PMMA/HDPE (70/30 w/w) blend with clay at different magnifications. TEM images at higher magnifications [Fig. 5(b,c)] clearly indicated the preferential location of the clay platelets in the PMMA matrix phase. The clay layers tended to disperse and locate mostly in the PMMA matrix in the PMMA/HDPE (70/30 w/w) blend because of the difference in polarity between PMMA and HDPE.

Furthermore, the morphology of the PMMA/HDPE (70/30 w/w) blend was not stable upon static annealing at 170°C for 4 h (Fig. 6). For instance, *D* (4.62 μm) of the PMMA/HDPE (70/30 w/w) blend [Fig. 6(a)] increased to about 6.75 μm after annealing [Fig. 6(d)], whereas *D* of the PMMA/HDPE (70/30 w/w) blend with 0.5 phr clay [Fig. 6(b)] and 1 phr PE-*g*-MA [Fig. 6(c)] did not change significantly after annealing [Fig. 6(e,f), respectively]. On the basis of this morphological analysis, we assumed that the intercalated clay layers in the PMMA matrix acted as a barrier that prevented the coalescence of the dispersed HDPE domains during melt mixing.

If this role of clay in reducing *D* of the dispersed phases in the PMMA/HDPE (70/30 w/w) blends is true, we cannot expect the same role of clay in another blend system where the clay layers are located in the domains only. Thus, we prepared PMMA/HDPE (30/70 w/w) blends without and with clay under the same blending conditions. As observed, the addition of 0.5 phr of clay in the reverse blend composition significantly increased *D*

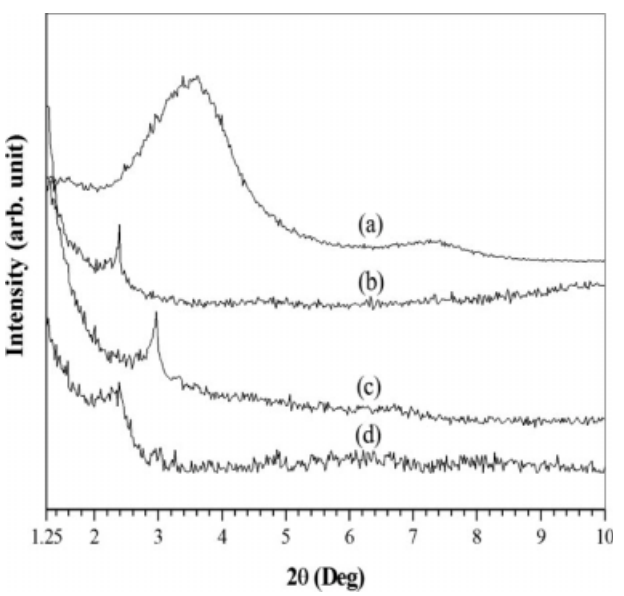

Figure 4 XRD patterns of (a) Cloisite 20A, (b) PMMA–clay, (c) HDPE–clay, and (d) PMMA/HDPE (70/30 w/w)–clay. The concentration of clay in all the nanocomposites was 1 phr.

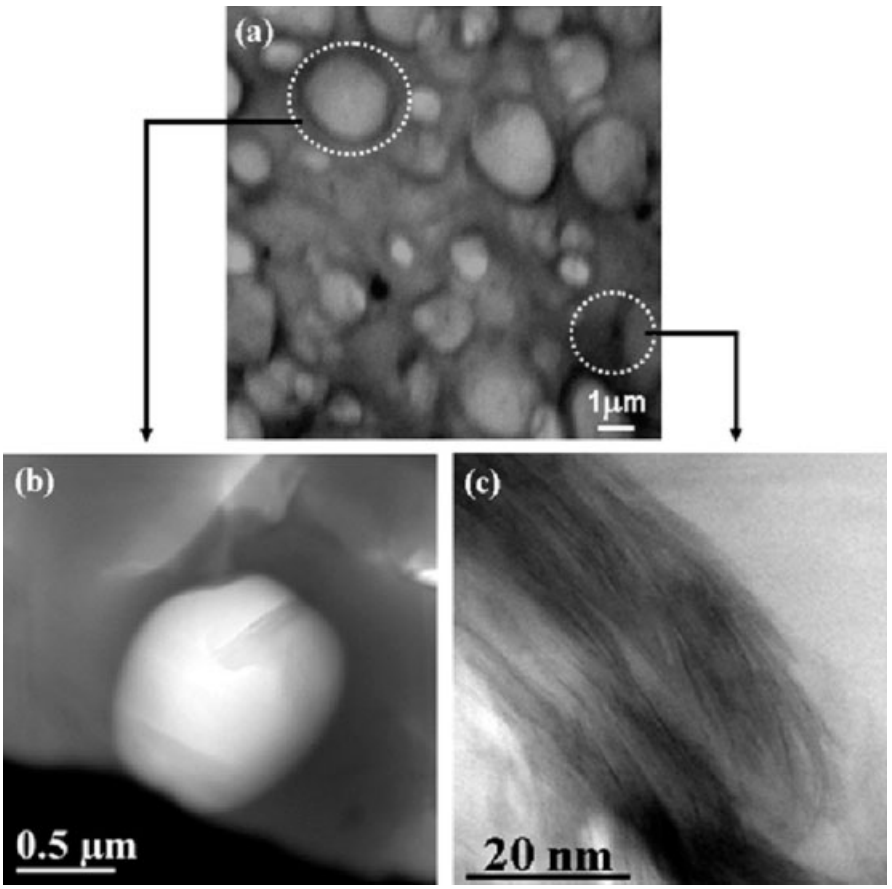

Figure 5 TEM images of the PMMA/HDPE (70/30 w/w) blend with 1 phr clay: (a) a lower magnification, (b) the HDPE domain at a higher magnification, and (c) the PMMA matrix at a higher magnification.

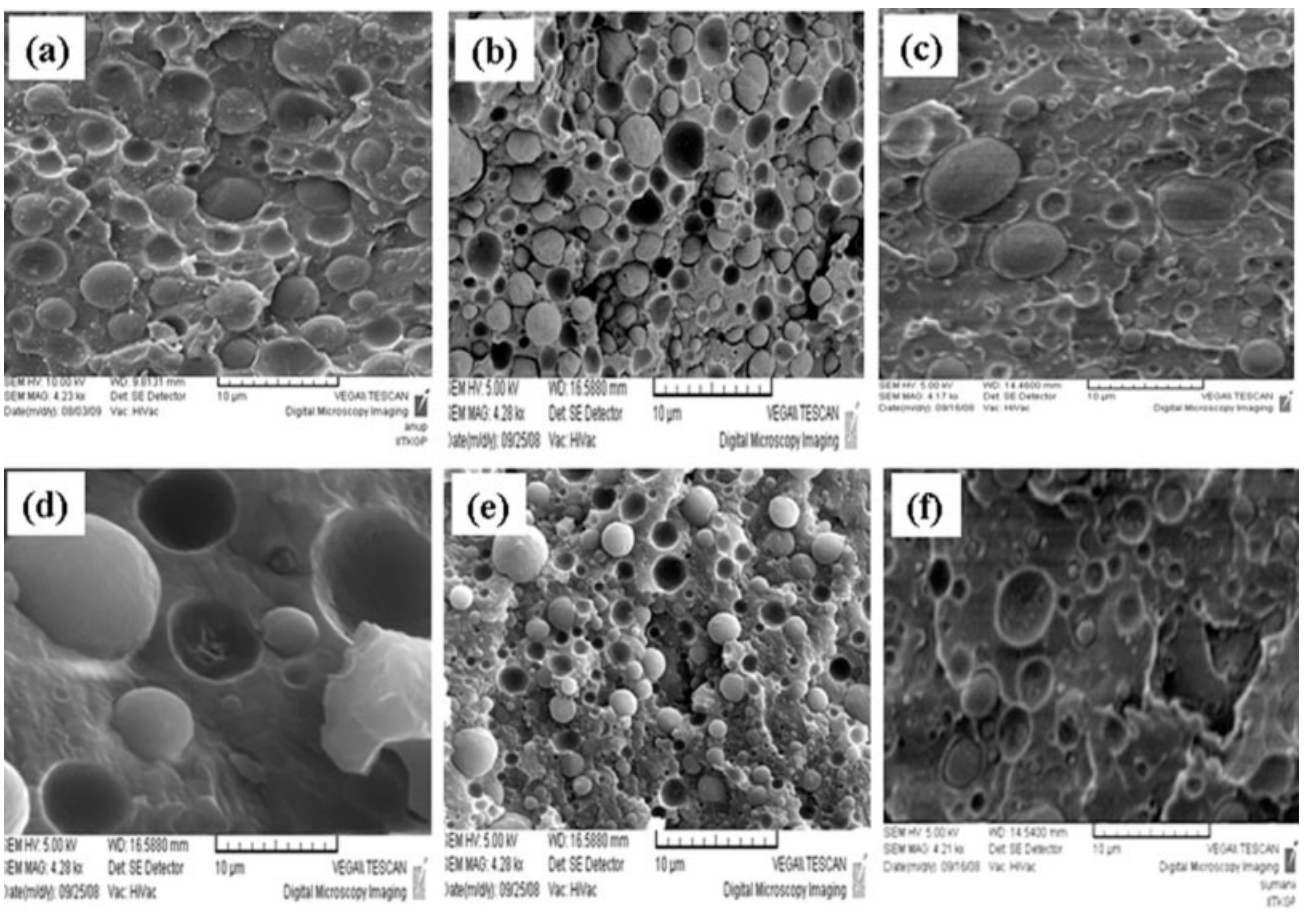

Figure 6 SEM images of PMMA/HDPE (70/30 w/w) blends (a–c) before and (d–f) after annealing at 170°C for 4 h: (a,d) the pure blend, (b,e) the blend with 0.5 phr clay, and (c,f) the blend with 1 phr PE-*g*-MA.

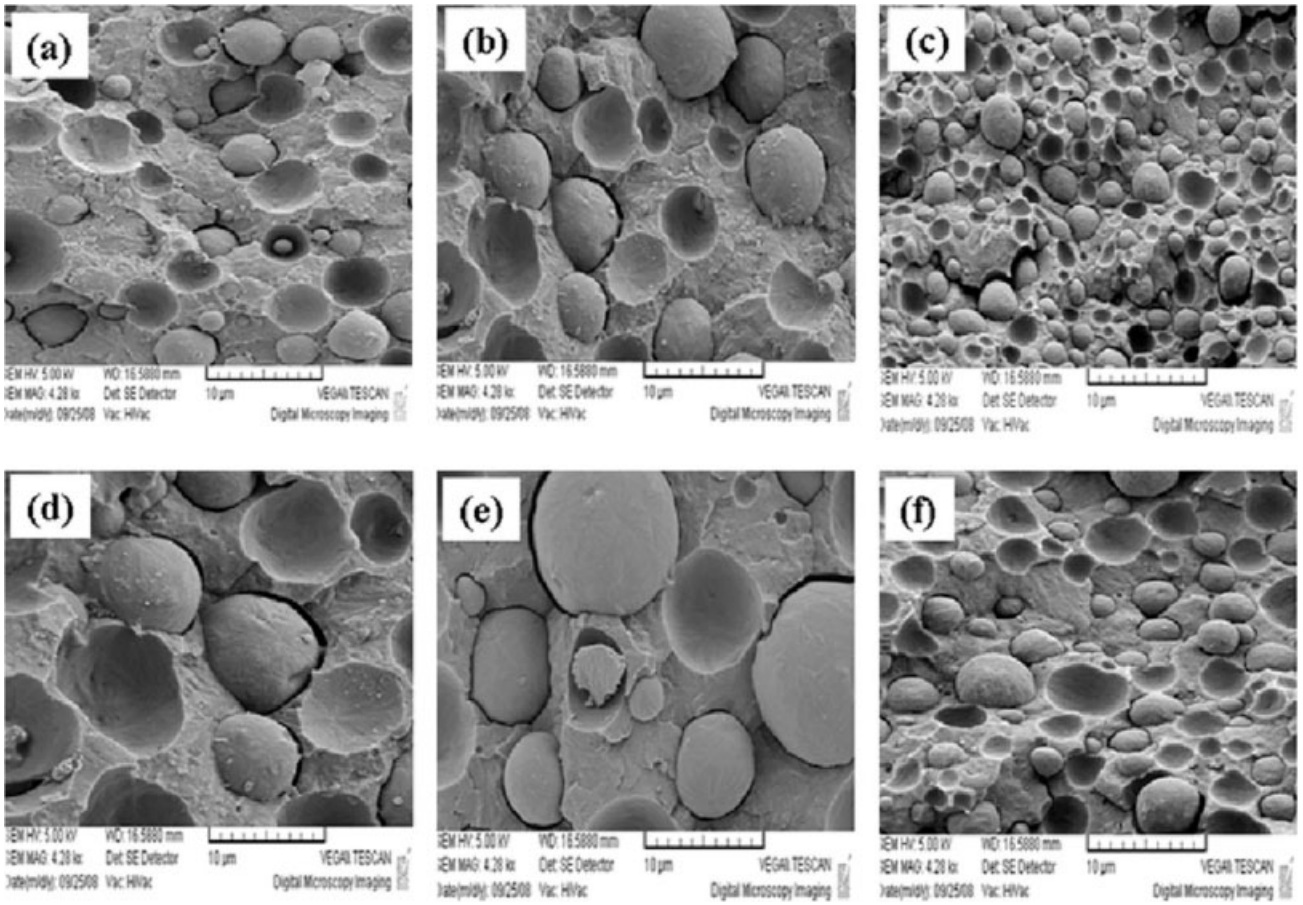

Figure 7 SEM images of PMMA/HDPE (30/70 w/w) blends (a–c) before and (d–f) after annealing at 170°C for 4 h: (a,d) the pure blend, (b,e) the blend with 0.5 phr clay, and (c,f) the blend with 1 phr PE-*g*-MA.

of the dispersed PMMA phase [Fig. 7(b)]. This was because of the preferential location of clay inside the PMMA domains, which increased the viscosity of the dispersed phase. However, the addition of PE-*g*-MA in the reverse blend decreased *D* of dispersed PMMA domains [Fig. 7(c)]. Again, the morphology of the PMMA/HDPE (30/70 w/w) blends without [Fig. 7(a)] and with 0.5 phr clay [Fig. 7(b)] was not stable upon static annealing [Fig. 7(d,e), respectively]. Thus, the absence of clay platelets in the HDPE matrix phase did not prevent the coalescence of the dispersed PMMA domains, whereas *D* of the

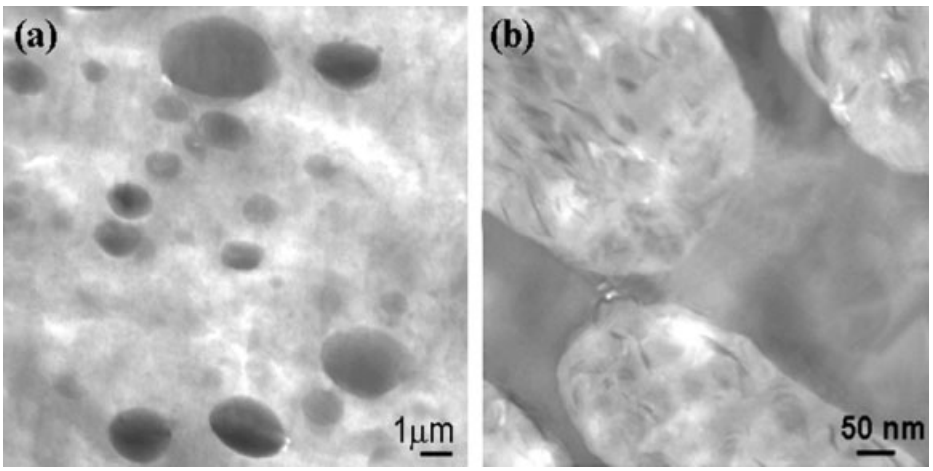

Figure 8 TEM images of the PMMA/HDPE (30/70 w/w) blend with 1 phr clay: (a) a lower magnification and (b) a higher magnification of the PMMA domains.

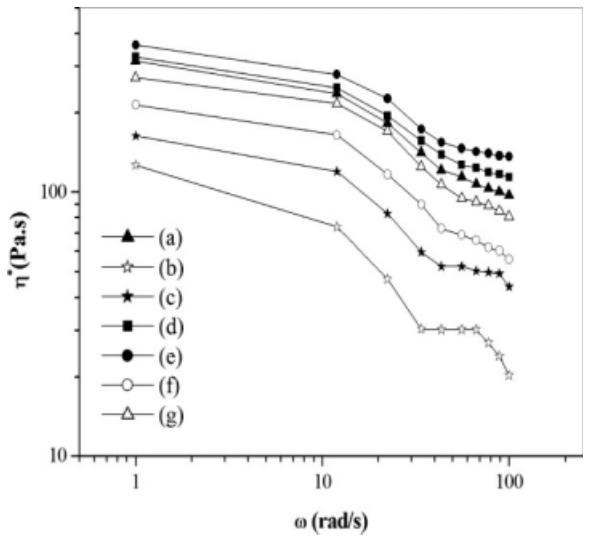

Figure 9 Plot of the complex viscosity (η*) versus the frequency (ω) at 210°C: (a) PMMA, (b) HDPE, (c) PMMA/HDPE (70/30 w/w), (d) PMMA–clay (0.7 phr), (e) PMMA-h, (f) PMMA/HDPE (70/30 w/w) blend with 0.5 phr clay, and (g) 70/30 (w/w) PMMA-h/HDPE blend without any clay.

dispersed phase in the reverse blend with 1 phr PE-*g*-MA [Fig. 7(c)] remained unaffected upon annealing [Fig. 7(f)]. This observation indicated that PE-*g*-MA acted as a compatibilizer for both PMMA/HDPE (70/30 w/w) and PMMA/HDPE (30/70 w/w) blends.

The location of the clay silicate layers in the PMMA/HDPE (30/70 w/w) blend, as investigated by TEM analysis, is shown in Figure 8. The dispersed PMMA phase in the blend appeared as black domains at lower magnification. TEM images at higher magnification clearly indicated the preferential location of the clay layers inside the dispersed PMMA domains in this reverse blend–clay nanocomposites system. Thus, in the reverse blend system, the absence of clay platelets in the matrix failed to prevent the coalescence of dispersed domains. Hence, no decrease in *D* of the dispersed phase was observed in the PMMA/HDPE (30/70 w/w) blend–clay composites.

The reduction in *D* of the dispersed HDPE phase in the PMMA/HDPE (70/30 w/w) blend–clay nanocomposites may have also stemmed from the increase in the matrix viscosity, as the clay platelets were selectively dispersed in the PMMA phase. Thus, in the PMMA/HDPE (70/30 w/w) blend with 0.5 phr clay selectively dispersed in the PMMA, the effective loading of clay in PMMA was 0.7 phr. We measured the complex viscosity of the neat PMMA, HDPE, PMMA–clay (0.7 phr), and PMMA/HDPE blends without and with clay (0.5 phr). As shown in Figure 9, the addition of 0.7 phr clay increased the melt viscosity of PMMA. Now, one can argue that the decrease in *D* in the PMMA/HDPE (70/30 w/w) blend may have been due to the increased viscosity of the PMMA in the presence of clay. To investigate the effect of matrix viscosity on the morphology, we also prepared the blend with another PMMA (PMMA-h) with a viscosity value higher than that of the PMMA–clay (0.7 phr) nanocomposites. The viscosity of the PMMA-h/HDPE (70/30 w/w) blend was also higher than that of the PMMA/HDPE (70/30 w/w) blend with 0.5 phr clay throughout the entire frequency range (0.1–100 rad/s). As observed, *D* of the dispersed phase in the PMMA-h/HDPE blend [Fig. 10(a)] was significantly lower than that of the PMMA/HDPE (70/30 w/w) blend without any clay [Fig. 1(a)]. However, the morphology of the PMMA-h/HDPE blends was not stable upon static annealing at 170°C for 4 h [Fig. 10(b)]. Interestingly, the *D* of the dispersed phase in PMMA/HDPE (70/30 w/w) blend with clay

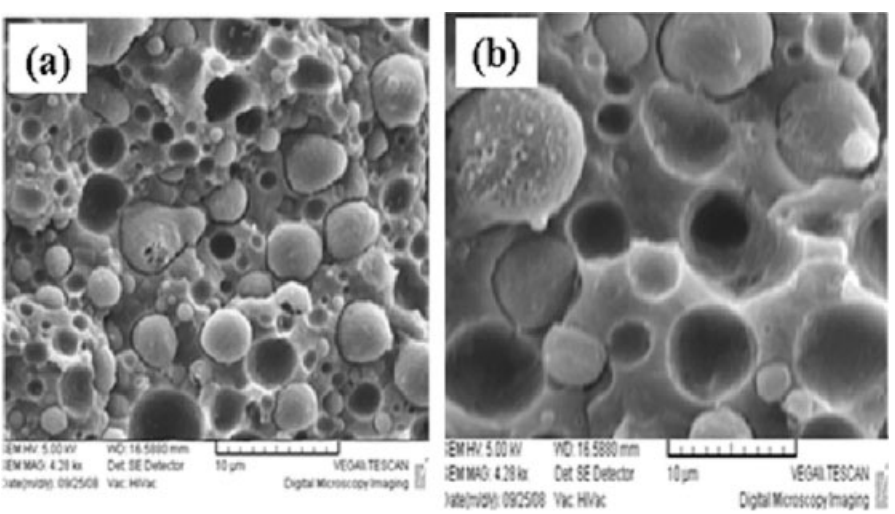

Figure 10 SEM images of PMMA-h/HDPE (70/30 w/w) blends (a) before and (b) after annealing.

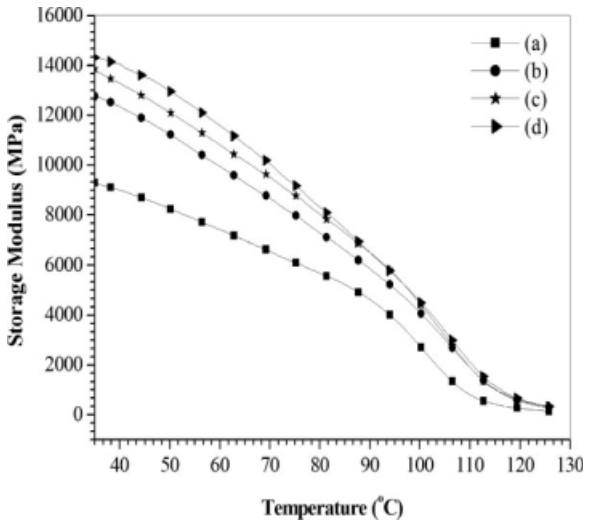

Figure 11 Storage modulus of PMMA/HDPE (70/30 w/w) blends with various amounts of clay: (a) 0, (b) 0.5, (c) 1, and (d) 3 phr.

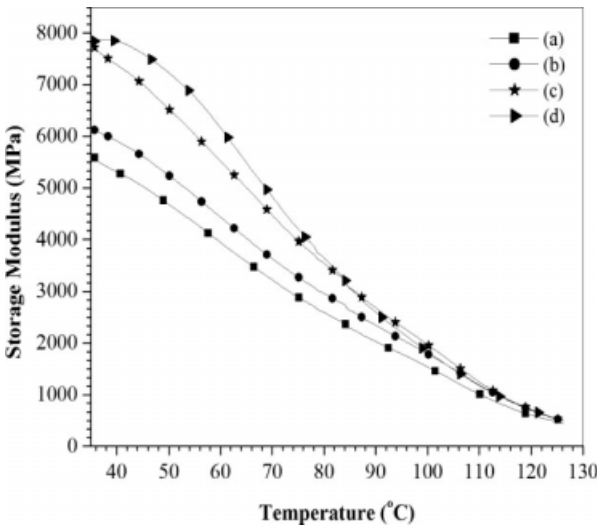

Figure 12 Storage modulus of PMMA/HDPE (30/70 w/w) blends with various amounts of clay: (a) 0, (b) 0.5, (c) 1, and (d) 3 phr.

(0.5 phr) was almost unaffected after it was annealed under the same conditions [Fig. 6(e)]. These observations clearly indicate that, as long as the clay platelets were dispersed in the matrix phase, they acted as a barrier to prevent the coalescence of dispersed domains.

Mechanical properties

The dynamic mechanical analysis results (Figs. 11 and 12) show that the storage modulus of the PMMA/HDPE (70/30 w/w and 30/70 w/w) blends increased with increasing clay content in the blends. However, the improvement of storage modulus of the blends with clay was more prominent in case of the PMMA/HDPE (70/30 w/w) blend. This was due to the presence of clay layers, mostly in the matrix PMMA phase, which increased the mixing efficiency by decreasing *D* of dispersed HDPE, and the reinforcing effect of the clay, which arose from the interaction with the PMMA (70 wt %). However, the preferential location of the clay inside the dispersed PMMA domains in the PMMA/HDPE (30/70 w/w) blend did not improve the mixing efficiency. Thus, the increase in the storage modulus in the presence of clay was a result of limited interactions between the clay layers and PMMA (30 wt %).

The tensile properties of the PMMA/HDPE (70/30 and 30/70 w/w) blends with clay and PE-*g*-MA are shown in Table I. The addition of PE-*g*-MA or clay increased the tensile strength of the blends. However, for a particular loading (1 phr), the extent of improvement in the tensile strength was more prominent with the clay. This could be explained by the presence of high-aspect-ratio stiff silicate layers in the polymer matrix, which resulted in a higher extent of interaction with the polymer chains. The elongation at break of all of the blends decreased with the addition of nanoclay. However, the improvement in the tensile strength for the reverse blend (30/70 w/w PMMA/HDPE) with nanoclay was not as prominent as it was with the PMMA/HDPE (70/30 w/w) blend. This was due to the location of clay mostly in the PMMA domains and a

TABLE I
Tensile Strength and Elongation at Break of PMMA/HDPE Blends with Different Amounts of Clay and PE-*g*-MA

Sample details	Tensile strength (MPa)	Elongation at break (%)
PMMA/HDPE (70/30 w/w)	11.0 ± 1.2	11 ± 2
PMMA/HDPE (70/30 w/w) with 0.5 phr clay	15.0 ± 1.5	9 ± 3
PMMA/HDPE (70/30 w/w) with 1 phr clay	25.0 ± 1.3	6 ± 2
PMMA/HDPE (70/30 w/w) with 0.5 phr PE-*g*-MA	13.0 ± 1.6	14 ± 2
PMMA/HDPE (70/30 w/w) with 1 phr PE-*g*-MA	19.0 ± 1.7	17 ± 2
PMMA/HDPE (30/70 w/w)	13.0 ± 1.5	11 ± 3
PMMA/HDPE (30/70 w/w) with 0.5 phr clay	16.0 ± 1.3	8 ± 2
PMMA/HDPE (30/70 w/w) with 1 phr clay	18.0 ± 1.4	5 ± 2

TABLE II
Thermal Properties of PMMA/HDPE Blends with Different Amounts of Nanoclay and PE-*g*-MA

Sample details	Degradation temperatures (°C)		
	T_{onset}	T_{50}	T_{max}
PMMA/HDPE (70/30 w/w)	346	385	481
PMMA/HDPE (70/30 w/w) with 0.5 phr clay	352	392	488
PMMA/HDPE (70/30 w/w) with 1 phr clay	356	397	495
PMMA/HDPE (70/30 w/w) with 3 phr clay	359	399	501
PMMA/HDPE (70/30 w/w) with 1 phr PE-*g*-MA	329	373	450
PMMA/HDPE (30/70 w/w)	320	383	458
PMMA/HDPE (30/70 w/w) with 1 phr clay	327	389	464
PMMA/HDPE (30/70 w/w) with 3 phr clay	346	406	514

T_{50} = temperature corresponding to the 50% weight loss; T_{max} = temperature corresponding to the maximum weight loss; T_{onset} = temperature corresponding to the onset of degradation.

minor amount of clay dispersed in the HDPE matrix in the reverse blend. The addition of nanoclay decreased the elongation at break of all of the blends, whereas the elongation properties of all of the blends with PE-*g*-MA increased, probably because of the adhesion of the polymers at the interface.

Thermal analysis

The thermal stability of the PMMA/HDPE (70/30 w/w and 30/70 w/w) blends with different amounts of clay was investigated with TGA. The temperatures corresponding to the onset of degradation, 50% weight loss, and maximum weight loss were calculated and are shown in Table II. The thermal stability of all the blends increased with the clay content. This indicated that an improvement in the thermal stability in the blend–clay nanocomposites depended on the extent of interaction between the polymer chains and the clay silicate layers, whereas addition of PE-*g*-MA in the PMMA/HDPE (70/30 w/w) blend decreased the thermal stability of the blend compared to that of the pure blend system; this was consistent with a previous report.[34]

CONCLUSIONS

This investigation showed the role of nanoclay on the morphology of PMMA/HDPE blends. The average D value of the dispersed HDPE phase in the PMMA/HDPE (70/30 w/w) blend decreased significantly even with lower loading (0.5 phr) of clay. For a particular loading, a reduction in the average dispersed domain diameter of the HDPE phase in the PMMA/HDPE blend was more prominent with nanoclay than that with PE-*g*-MA. The X-ray diffraction study and microscopic analysis of the PMMA/HDPE (70/30 w/w) blends with clay indicated selective location of the intercalated clay layers in the matrix phase. Thus, the intercalated clay platelets dispersed in the matrix phase acted as a barrier, which prevented the coalescence of the dispersed phases during melt mixing.

References

1. Folkes, M. J.; Hope, P. S. Polymer Blends and Alloys; Chapman & Hall: London, 1993.
2. Utracki, L. A. Polymer Alloys and Blends; Hanser: Munich, 1989.
3. Creton, C.; Kramer, E. J.; Hui, C. Y.; Brown, H. R. Macromolecules 1992, 25, 3075.
4. Kim, S.-J.; Shin, B.-S.; Hong, J.-L.; Cho, W.-J.; Ha, C.-S. Polymer 2001, 42, 4073.
5. Boucher, E.; Folkers, J. P.; Hervet, H.; Leger, L.; Creton, C. Macromolecules 1996, 29, 774.
6. Wang, T.; Liu, D.; Xiong, C. J Mater Sci 2007, 42, 3398.
7. Pinnavaia, T. J.; Beall, G. W. Polymer–Clay Nanocomposites; Wiley: New York, 2000.
8. Alexandre, M.; Dubois, P. Mater Sci Eng 2000, 28, 1.
9. Sinha Ray, S.; Okamoto, M. Prog Polym Sci 2003, 44, 7427.
10. Dennis, H. R.; Hunter, D. L.; Chang, D.; Kim, S.; White, J. L.; Cho, J. W. Polymer 2001, 42, 9513.
11. Manias, E.; Touny, A.; Wu, L.; Strawhecker, K.; Lu, B.; Chung, T. C. Chem Mater 2001, 13, 3516.
12. Sohn, J. I.; Lee, C. H.; Lim, S. T.; Kim, T. H.; Choi, H. J.; Jhon, M. S. J Mater Sci 2003, 38, 1849.
13. Zhang, G.; Shichi, T.; Takagi, K. Mater Lett 2003, 57, 1858.
14. Rhutesh, K. S.; Paul, D. R. Polymer 2004, 45, 2991.
15. Acierno, D.; Scarfato, P.; Amándola, E.; Nocerino, G.; Costa, G. Polym Eng Sci 2004, 44, 1012.
16. Peeterbroeck, S.; Alexandre, M.; Jerome, R.; Dubois, P. Polym Degrad Stab 2005, 90, 288.
17. Zou, H.; Zhang, Q.; Tan, H.; Wang, K.; Du, R.; Fu, Q. Polymer 2006, 47, 6.
18. Hong, J. S.; Namkung, H.; Ahn, K. H.; Lee, S. J.; Kim, C. Polymer 2006, 47, 3967.
19. Gelfer, M. Y.; Hyun, H. S.; Liu, L.; Benjamin, S. H.; Benjamin, C.; Rafailovich, M.; Mayu, S.; Vladimir, Z. J Polym Sci Part B: Polym Phys 2003, 41, 44.
20. Wang, Y.; Zhang, Q.; Fu, Q. Macromol Rapid Commun 2003, 24, 231.
21. Sinha Ray, S.; Bousmina, M. Macromol Rapid Commun 2005, 26, 450.

22. Sinha Ray, S.; Bousmina, M. Macromol Rapid Commun 2005, 26, 1639.
23. Sinha Ray, S.; Pouliot, S.; Bousmina, M.; Utracki, L. A. Polymer 2004, 45, 8403.
24. Sinha Ray, S.; Bandyopadhyay, J.; Bousmina, M. Macromol Mater Eng 2007, 209, 729.
25. Khatua, B. B.; Lee, D. J.; Kim, H. Y.; Kim, J. K. Macromolecules 2004, 37, 2454.
26. Gcwabaza, T.; Ray, S. S.; Focke, W. W.; Maity, A. Eur Polym J 2009, 45, 353.
27. Martins, C. G.; Larocca, N. M.; Paul, D. R.; Pessan, L. A. Polymer 2009, 50, 1743.
28. Baghaei, B.; Jafari, S. H.; Khonakdar, H. A.; Rezaeian, I.; As'habi, L.; Ahmadian, S. Polym Bull 2009, 62, 255.
29. Calcagno, C. I. W.; Mariani, C. M.; Teixeira, S. R.; Mauler, R. S. Compos Sci Technol 2008, 68, 2193.
30. Li, Y.; Shimizu, H. Polymer 2004, 45, 7381.
31. Li, Y.; Shimizu, H. Macromol Rapid Commun 2005, 26, 710.
32. Filippone, G.; Dintcheva, N. T.; Acierno, D.; Mantia, F. P. L. Polymer 2008, 49, 1312.
33. Favis, B. D. Polymer 1994, 35, 1552.
34. Modesti, M.; Lorenzetti, A.; Bon, D.; Besco, S. Polym Degrad Stab 2006, 91, 672.